Attractive photons in a quantum nonlinear medium

Citation: Firstenberg, Ofer, Thibault Peyronel, Qi-Yu Liang, Alexey V. Gorshkov, Mikhail D. Lukin, and Vladan Vuletic. "Attractive Photons in a Quantum Nonlinear Medium." Nature 502, no. 7469 (September 25, 2013): 71–75.

As Published: http://dx.doi.org/10.1038/nature12512

Publisher: Nature Publishing Group

Persistent URL: http://hdl.handle.net/1721.1/91605

Version: Author's final manuscript: final author's manuscript post peer review, without publisher's formatting or copy editing

Attractive Photons in a Quantum Nonlinear Medium

Ofer Firstenberg*[1], Thibault Peyronel*[2], Qi-Yu Liang[2], Alexey V. Gorshkov[3], Mikhail D. Lukin[1], and Vladan Vuletić[2]
[1]*Department of Physics, Harvard University, Cambridge, MA, 02138*
[2]*Department of Physics and Research Laboratory of Electronics, Massachusetts Institute of Technology, Cambridge, MA 02139, USA*
[3]*Institute for Quantum Information and Matter, California Institute of Technology, Pasadena, CA 91125, USA and*
** These authors contributed equally to this work*

The fundamental properties of light derive from its constituent particles (photons) that are massless and do not interact with one another[1]. At the same time, it has been long known that the realization of coherent interactions between individual photons, akin to those associated with conventional massive particles, could enable a wide variety of unique scientific and engineering applications[2,3]. Here, by coupling light to strongly interacting atomic Rydberg states in a dispersive regime, we demonstrate a quantum nonlinear medium inside which individual photons travel as massive particles with strong mutual attraction, such that the propagation of photon pairs is dominated by a two-photon bound state[4–7]. We measure the dynamical evolution of the two-photon wavefunction using time-resolved quantum state tomography, and demonstrate a conditional phase shift[8] exceeding one radian, resulting in polarization-entangled photon pairs. Unique applications include all-optical switching, deterministic photonic quantum logic, and the generation of strongly correlated states of light[9].

Interactions between individual photons are being explored in cavity quantum electrodynamics, where a single, confined electromagnetic mode is coupled to an atomic system[10–12]. Our approach is to couple a light field propagating in a dispersive medium to highly excited atomic states with strong mutual interactions (Rydberg states)[13,14]. Similar to previous studies of quantum nonlinearities via Rydberg states that were based on dissipation[15–19] rather than dispersion[20], we make use of electromagnetically induced transparency (EIT) to slow down the propagation of light[21] in a cold atomic gas. By operating in a dispersive regime away from the intermediate atomic resonance (Fig. 1b), where atomic absorption is low and only weakly nonlinear[22], we realize a situation where Rydberg-atom-mediated coherent interactions between individual photons dominate the propagation dynamics of weak light pulses. Previous theoretical studies have proposed various scenarios for inducing strong interactions between individual photons[2,3,23] and for creating bound states of a few quanta[4,5,7,24], a feature generic to strongly interacting quantum field theories. The first experimental realization of a photonic system with strong attractive interactions, including evidence for a predicted two-photon bound state, represents the main result of this work.

Our experiment (outlined in Fig. 1a) makes use of an ultracold rubidium gas loaded into a dipole trap, as described previously[19]. The probe light of interest is σ^+ polarized, coupling the ground state $|g\rangle$ to the Rydberg state $|r\rangle$ via an intermediate state $|e\rangle$ of linewidth $\Gamma/(2\pi) = 6.1$ MHz by means of a control field that is detuned by Δ below the resonance frequency of the upper transition $|e\rangle \to |r\rangle$ (Fig. 1b). Under these conditions, for a very weak probe field with mean incident photon rate $R_i = 0.5\ \mu\text{s}^{-1}$, EIT is established when the probe detuning matches that of the control field (see Fig. 1c showing the probe transmission and phase shift). However, the Rydberg medium is extremely nonlinear: a probe photon rate of $R_i = 5\ \mu\text{s}^{-1}$ saturates the medium due to the Rydberg blockade[25], yielding a probe spectrum close to the bare two-level response. Given the measured system bandwidth of about 5 μs^{-1}, this implies a substantial nonlinear response with average pulse energies corresponding to less than one photon per inverse bandwidth. We perform our experiments on two-photon resonance $|g\rangle \to |r\rangle$, where the transmission is approximately independent of the probe photon rate for our experimental parameters at $|\Delta| > \Gamma$, yielding a purely dispersive nonlinearity. The linear dispersion at this point corresponds to a reduced probe group velocity of typically $v_g = 400$ m/s, while the group velocity dispersion endows the photons with an effective mass[26] $m \approx 1000\hbar\omega/c^2$, where ω is the optical frequency and c is the speed of light in vacuum.

In order to explore the quantum dynamics in the propagation of photon pairs, we measure time-dependent two-photon correlation functions of the transmitted light (see Fig. 1a). To determine both amplitude and phase of the σ^+-polarized probe field, we prepare input coherent light in a linearly polarized state $|V\rangle = (|\sigma^+\rangle + |\sigma^-\rangle)/\sqrt{2}$, where the σ^- component (approximately non-interacting due to the 15-fold smaller transition strength) serves as a phase reference. To analyze the properties of photon-pairs, we measure two-photon correlation functions $g^{(2)}_{\alpha\beta}$ in different polarization bases α, β (Fig. SI3). The component $g^{(2)}_{++}$ directly gives the probability density of the σ^+-polarized interacting photon pairs. Figure 1d shows $g^{(2)}_{++}$ for a control detuning $\Delta/(2\pi) = 14$ MHz as a function of the time separation $\tau = t_1 - t_2$ between the photons detected at times t_1, t_2, converted into a relative distance in the medium via the group velocity v_g. A

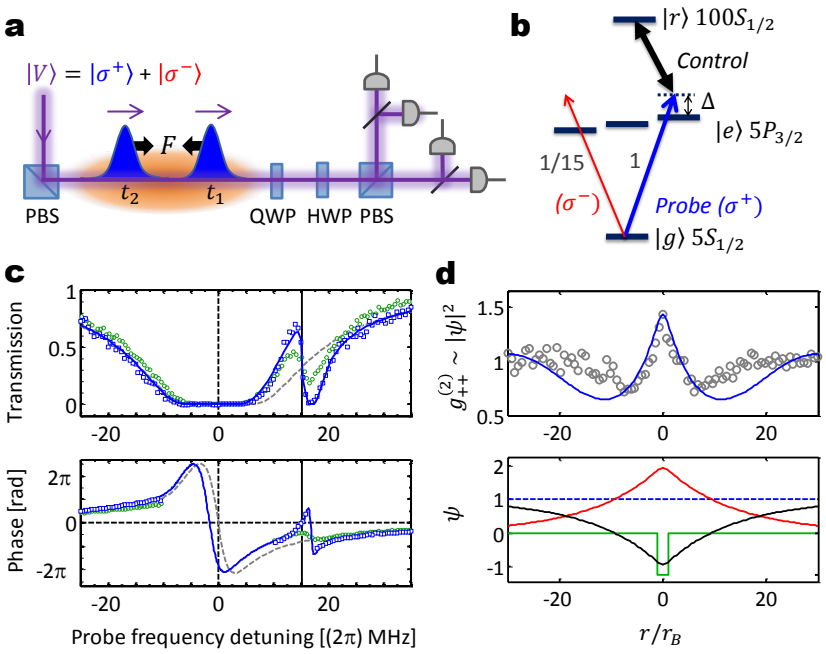

FIG. 1: **Photons exhibiting strong mutual attraction in a quantum nonlinear medium. a,b,** A linearly polarized weak laser beam near the transition $|g\rangle \rightarrow |e\rangle$ at 780 nm is sent into a cold rubidium gas driven by a control laser near the transition $|e\rangle \rightarrow |r\rangle$ at 479 nm. Strong nonlinear interactions between σ^+-polarized photons are detected via photon-photon correlation functions of the transmitted light for a set of different polarization bases, as determined by a quarter-waveplate (QWP), a half-waveplate (HWP), and a polarizing beam-splitter (PBS). Here σ^- photons serve as a phase reference. **c,** Transmission spectra (top) and phase shift (bottom) for σ^+ photons with incoming rate of $R_i = 0.5\ \mu s^{-1}$ (blue squares) and $R_i = 5\ \mu s^{-1}$ (green circles), for a control field red-detuned by $\Delta/(2\pi) = 15$ MHz (blue line is theory). The spectrum at high probe rate approaches that of the undriven two-level system (dashed gray; see also Fig. SI2). The solid vertical line corresponds to the EIT resonance. **d,** Photon bunching and two-photon bound state. Theoretically predicted photon-photon correlation function in the Schroedinger-equation approximation (top, blue line) for $\Delta/(2\pi) = 14$ MHz, with a potential well of width $2r_B$ (bottom, green line). The bound state (bottom, red) and the superposition of scattering states (bottom, black) form the initial wave function $\psi = 1$ (bottom, dashed blue). The two-photon bound state results in the observed bunching in the correlation function $g^{(2)}_{++} \sim |\psi|^2$ (top, gray circles), where time has been converted into distance via the group velocity v_g. The boundary effects resulting from the finite extent of the atom cloud become important for $|r| \geq 5\ r_B$.

prominent feature is the cusp at $r = v_g\tau = 0$, which is characteristic of a predicted two-photon bound state[5,7], as discussed below.

The measured $g^{(2)}_{\alpha\beta}$ allow us to reconstruct the two-photon density matrix ρ using quantum state tomography via a maximum-likelihood estimation[27,28], from which we define an interaction matrix $\tilde{\rho}$ by factoring out the linear response, such that $\tilde{\rho}$ directly quantifies the nonlinearity (see Methods). The density matrix approach is necessary to account for decoherence and technical imperfections. The probability density of two interacting σ^+ photons, $g^{(2)}_{++} = \tilde{\rho}_{++,++}$, and the nonlinear phase, acquired by the $\sigma^+\sigma^+$ pair relative to a non-interacting $\sigma^-\sigma^-$ pair, $\phi = \arg[\tilde{\rho}_{++,--}]$, are shown in Figs. 2a,b for $\Delta/(2\pi) = 14$ MHz. The time dependence allows us to extract the nonlinear phase as a function of the photon-photon separation. Clearly visible is the bunching of photons, *i.e.* an increased probability for photons to exit the medium simultaneously ($t_1 \approx t_2$), and a substantial nonlinear two-photon phase shift of -0.5 rad in that region. Figure 2c shows the intensity correlation in the dissipation-dominated antibunching regime[19] at $\Delta = 0$ and in the dispersive regime at $|\Delta| > \Gamma$ exhibiting bunching, and Fig. 2d displays the nonlinear phase for two different detunings. The transition from the dissipative to the dispersive regime is summarized in Figs. 3a,b. In the dispersive regime, the nonlinear phase shift $\phi(\tau = 0)$ can reach $(-0.32 \pm 0.02)\pi$, at a detuning $\Delta/(2\pi) = 9$ MHz and a linear transmission of order 50%. The observed signal exhibits asymmetries under a sign change of the detuning Δ from the intermediate atomic $|e\rangle$ state, particularly in the nonlinear phase ϕ.

The origin of the quantum nonlinearity underlying these observations is explained by the following simple model. The repulsive Van-der-Waals interaction be-

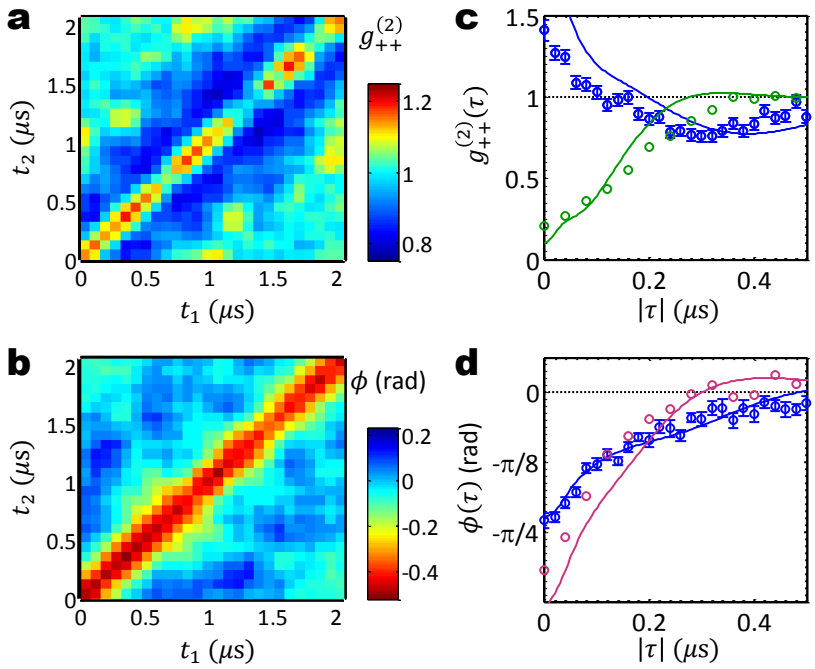

FIG. 2: **Propagation of interacting photon pairs.** Measured second-order correlation function (**a**) and nonlinear phase shift (**b**) of interacting photon pairs at $\Delta = 2.3\Gamma$. The photons are detected at times t_1 and t_2. (**c**) Second-order correlation function displayed as a function of the time difference $|\tau| = |t_1 - t_2|$ between the photons, showing the transition from anti-bunching on resonance ($\Delta = 0$, green) to bunching at large detuning ($\Delta = 2.3\Gamma$, blue). Points are experimental data, lines are full numerical simulations. All $g^{(2)}_{++}$ measurements are rescaled by their value at $\tau > 1.5$ μs (See SI). (**d**) Nonlinear phase-shift versus $|\tau|$ for two different detunings ($\Delta = 1.5\Gamma$, purple, and $\Delta = 2.3\Gamma$, blue). The 1σ error is ± 30 mrad, dominated by photon shot noise.

tween two Rydberg atoms $V(r) = \hbar C_6/r^6$ tunes the doubly excited Rydberg state far off EIT resonance for distances $|r| < r_B$, where $r_B = \sqrt[6]{C_6/\gamma}$ is the Rydberg blockade radius[14,29,30], C_6 the van der Waals coefficient, $\gamma = \Omega_c^2/|4\Delta|$ is the EIT linewidth at detuning $|\Delta| \gg \Gamma$, and Ω_c the Rabi frequency of the control field. While for photons with large separation in the medium $|r| > r_B$, the phase shift that would originate from the bare $|g\rangle \to |e\rangle$ probe transition is suppressed by EIT, for small photon separations $|r| \leq r_B$, the light acquires this phase shift (see Fig. 1c). This explicit dependence of the refractive index upon photon-photon separation can be modeled in one dimension as a potential well with a characteristic width of $2r_B$. Qualitatively, a substantial two-photon phase shift arises for $\frac{r_B}{l_a}\frac{\Gamma}{|\Delta|} \gtrsim 1$, where l_a is the resonant attenuation length in the medium, *i.e.* for sufficiently high atomic density. Furthermore, the probe field must also be transversally compressed to a waist size $w < r_B$ to ensure interactions. For our parameters using the Rydberg state $100S_{1/2}$ and $\Omega_c/(2\pi) = 10$ MHz, we have $r_B \cong 18\,\mu$m at detunings of a few Γ, $l_a = 4\,\mu$m at the peak density, and $w = 4.5\,\mu$m, fulfilling the conditions for strong interactions for $|\Delta| \lesssim 5\Gamma$.

The propagation of σ^+-polarized photon pairs in such a medium can be understood by first considering an idealized situation with no decoherence between the Rydberg state and the ground state. Then the steady-state in a one-dimensional homogenous medium can be described by a two-photon wavefunction $\psi(z_1, z_2)$, whose evolution is approximately governed by a simple equation[19] in the center-of-mass $R = (z_1 + z_2)/2$ and relative $r = z_1 - z_2$ coordinates:

$$i\partial_R\psi = 4l_a\left[i + \frac{2\Delta}{\Gamma} - \mathcal{V}(r)\frac{\Omega_c^2}{\Gamma^2}\right]\partial_r^2\psi + \frac{\mathcal{V}(r)}{l_a}\psi. \qquad (1)$$

Here the effective potential $\mathcal{V}(r) = [i + 2\frac{\Delta}{\Gamma}(1 + 2r^6/r_B^6)]^{-1}$ approaches $(i + 2\Delta/\Gamma)^{-1}$ inside the blockaded volume ($|r| < r_B$), and zero outside. The solution relates to our measurements in the time domain for small $|\tau|$ approximately via $\psi(R = L, r = v_g\tau) \sim \sqrt{g^{(2)}_{++}(\tau)}e^{i\phi(\tau)}$ (see SI for the exact relation). Far off resonance ($|\Delta| \gg \Gamma, \Omega_c$), Eq. (1) corresponds to a Schroedinger equation with the center-of-mass propagation distance R playing the role of effective time. The photons' effective mass $m \propto -\Gamma/(16l_a\Delta)$ can be positive or negative depending on the sign of the detuning Δ. As the sign of the potential also changes with Δ (potential well for $\Delta < 0$, barrier for $\Delta > 0$), the effective force (F in Fig. 1a) in both

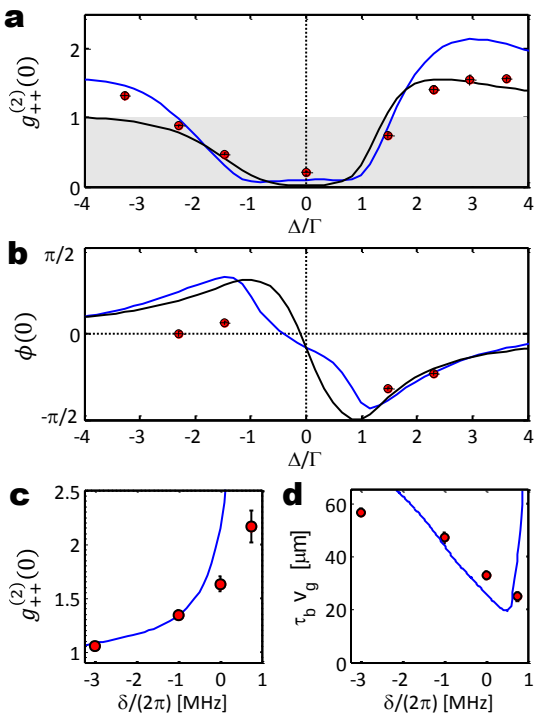

FIG. 3: **Detuning dependence of the photon-photon interaction.** Equal-time two-photon correlation $g^{(2)}_{++}(0)$ (**a**) and nonlinear phase $\phi(0)$ (**b**) versus detuning Δ from the intermediate state $|e\rangle$. Blue lines are full theoretical simulations, while black lines are the result of the Schrodinger-equation approximation, assuming a simplified delta-function potential. Vertical error bars represent 1σ and horizontal error bars are ± 0.5 (2π) MHz. Equal-time correlation function (**c**) and spatial extent of the bunching feature (**d**) versus Raman detuning δ from the EIT resonance $|g\rangle \rightarrow |r\rangle$ for $\Delta = 3\Gamma$, showing increased photon-photon attraction due to a deeper potential near Raman resonance. The characteristic bunching-timescale τ_b is the half-width of the cusp feature of $g^{(2)}_{++}$, defined at half-height between the peak value at $\tau = 0$ and the local minimum closest to $\tau = 0$. In (**c,d**), error bars correspond to $\pm 1\sigma$. The theoretical model (solid line) breaks down close to the Raman resonance at $\delta = 1.3$ (2π) MHz $\approx \Omega_c^2/(4\Delta)$, where the single-photon component of the probe field is strongly absorbed.

cases is attractive and the resulting dynamics similar (see SI). However, the potential for $\Delta < 0$ also exhibits additional features near the edges of the well, corresponding to a Raman resonance $|g\rangle \rightarrow |r\rangle$ for the interaction-shifted Rydberg state at some interatomic distance near $|r| = r_B$. These features are likely responsible for the deviation from (anti-)symmetry under the change of the sign of Δ displayed in Figs. 3a,b.

In the experimentally relevant regime, the effective potential supports only one bound-state $\psi_B(r)$ depicted in Fig. 1d. The initial wavefunction $\psi(R = 0, r) = 1$ is a superposition of $\psi_B(r)$ and the continuum of scattering states. The accumulation of probability near $r = 0$ can then be understood as arising from the interference between the bound and scattering states that evolve at different frequencies, and the observed bunching feature in $g^{(2)}_{++}$ reflects the wavefunction of the two-photon bound state (see SI). As shown in Figs. 3a,b, the solution of the Schroedinger-like equation (1) with a simplified delta-function potential captures the essential features of the nonlinear two-photon propagation. Additional experimental evidence for the bound-state dynamics is obtained by tuning the probe field relative to the EIT resonance, thereby varying the strength of the two-photon interaction potential. As the probe detuning approaches the Raman resonance, the difference in refractive indices inside and outside the blockade radius increases and the potential deepens (see SI and Fig. 1c). Consequently, the bound state becomes more localized and the bunching, quantified by $g^{(2)}_{++}(0)$, is enhanced, as evidenced in Figs. 3c,d. Note that the size of the two-photon bound state and correspondingly the width of the bunching feature $2\tau_b v_g \sim 70$ μm, exceed the width of the potential well of $2r_B \sim 35$ μm, as expected for a potential with one weakly bound state.

Figures 2 and 3 also show the results of our full theoretical model, in which we numerically solve the set of propagation equations for the light field and atomic coherences. The model incorporates the longitudinal atomic-density distribution and the decoherence of the Rydberg state (see SI for details). These simulations are in good agreement with our experimental results and the predictions of the simplified model, Eq. (1), confirming that the evolution of the two-photon wavepacket is dominated by the attractive force between the photons.

Finally, we study the quantum coherence and polarization properties of the transmitted photon pairs. Figure 4a compares the purity of the two-photon density matrix $\rho(\tau)$, that includes photon interactions, to the purity of the product of one-photon matrices $\rho^{(1)} \otimes \rho^{(1)}$ for non-interacting photons. At large photon separation τ, the purity $P(\tau)$ of the two-photon density matrix is dominated by the one-photon decoherence due to partial depolarization of the transmitted light (see SI). This depolarization is attributed to the difference in group delay τ_d between the σ^+ and the faster σ^- photons ($\tau_d^{\sigma^+} - \tau_d^{\sigma^-} = 280$ ns) that is not negligible compared to the coherence time of the probe laser (650 ns). At the same time, σ^+ photons bound to each other travel faster and are more robust against this decoherence mechanism, as evidenced by the greater purity at small τ. Even in the presence of this depolarization, the coherent nonlinear interaction in the dispersive medium produces entanglement in the outgoing polarization state of two photons. We quantify the degree of polarization entanglement by a time-dependent concurrence $C(\tau)$ (see Fig. 4b and SI). The obtained value $C(0) = 0.09 \pm 0.03$ clearly indicates deterministic entanglement of previously independent photons upon passage through the quantum nonlinear medium. The measured value is in reasonable agreement with the theoretical prediction $C_{\rm th}(0) = 0.13$, calculated for a con-

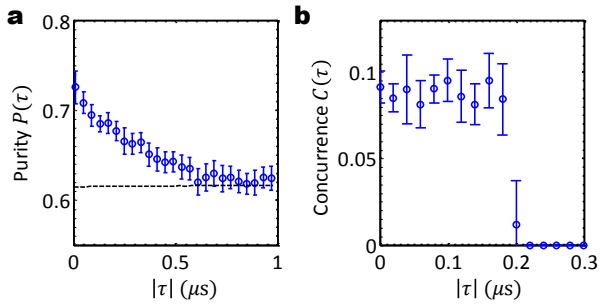

FIG. 4: **Quantum coherence and entanglement. a,** Purity $P(\tau) = \mathrm{Tr}[\rho(\tau)^2]$ of the measured two-photon density-matrix ρ for $\Delta = 2.3\Gamma$ (blue symbols), approaching at large photon separation the purity expected from the measured one-photon density-matrix $\mathrm{Tr}[(\rho^{(1)} \otimes \rho^{(1)})^2]$ (dotted black line). Interacting $\sigma^+\sigma^+$ photon pairs near $\tau = 0$ exhibit lower decoherence. Error bars (1σ) are derived from the uncertainty in the density matrix due to detection shot noise. **b,** Concurrence $C(\tau)$ calculated from ρ, indicating polarization entanglement of proximal photons upon transmission through the quantum nonlinear medium.

ditional phase $\phi(0) = \pi/4$, a purity $P(0) = 0.73$, and 50% σ^+ linear transmission.

In our experiment, the transmission and achievable nonlinear phase are limited by the available control-field intensity, laser linewidth, and atomic motion. These technical limitations can be circumvented by using stronger control lasers with improved frequency stability and colder atomic clouds trapped in both ground and Rydberg states. While in our present system the non-linear phase would not be uniformly acquired by a bandwidth-limited two-photon pulse, a high fidelity two-photon phase-gate may be achievable using, *e.g.*, a counter-propagating geometry and higher optical depths[14].

The realization of coherent, dispersive photon-photon interactions opens up several new research directions. These include the exploration of a novel quantum matter composed from strongly interacting, massive photons[9]. Measurements of higher-order correlation functions may give direct experimental access to quantum solitons composed of a few interacting bosons[24], or to the detection of crystalline states of a photonic gas[9]. By colliding two counterpropagating photons, it may be possible to imprint a spatially homogeneous phase shift of π on the photon pair, corresponding to a deterministic quantum gate[14] for scalable optical quantum computation[13]. Finally, by accessing other Rydberg states via, *e.g.*, microwave transitions, it may become possible to control the state of multi-photon pulses with just one quantum of light, thereby realizing a single-photon transistor[6] for applications in quantum networks, and the creation of multi-photon entangled states.

Methods

The experimental setup is detailed in Ref. [19], with the following modifications. The dipole trap is periodically switched off with a 5.5 μs half-period, and the measurements are performed during the dark time to avoid inhomogeneous broadening. Photons detected in the first 1.5 μs after the turn-off of the dipole trap are not included in the analysis, to guarantee steady-state EIT. For each experimental cycle, data is accumulated over 400 periods of the dipole-trap modulation. The trapped atomic cloud has a longitudinal r.m.s. length of $\sigma_{ax} = 36$ μm and a peak density of $\rho_0 = 10^{12}$ atoms cm^{-3}. The average resonant optical depth is 22, with less than 20% variation over the measurement time. The probe and control beams are counter-propagating in order to reduce the residual Doppler broadening to 50 (2π) kHz. Linearly polarized probe laser light enters the medium at an average photon rate of 1.6 μs^{-1}. Quarter- and half-waveplates at angles q and h, respectively, followed by a polarizing beam splitter, project the outgoing probe light onto a chosen polarization basis (see Fig. 1a). Four single-photon counting modules measure the pair correlation events at times t_1 and t_2. Normalized second-order correlation functions $g^{(2)}_{\alpha\beta}$ are calculated using the photon coincidence counts between the different detectors and the average count rates. The time bins [80 ns for $g^{(2)}_{\alpha\beta}(t_1, t_2)$ and 20 or 40 ns for $g^{(2)}_{\alpha\beta}(\tau)$] were chosen to capture the temporal dynamics of the correlation functions with reasonable signal-to-noise ratio.

In the quantum-state tomography, we numerically optimize a Hermitian, positive semidefinite, two-photon density-matrix,

$$\rho = \begin{pmatrix} \rho_{++,++} & \rho_{++,S} & \rho_{++,--} & 0 \\ \rho_{S,++} & \rho_{S,S} & \rho_{S,--} & 0 \\ \rho_{--,++} & \rho_{--,S} & \rho_{--,--} & 0 \\ 0 & 0 & 0 & \rho_{A,A} \end{pmatrix}$$

in the two-qubit basis $\{|\sigma_1^+\sigma_2^+\rangle, |S\rangle, |\sigma_1^-\sigma_2^-\rangle, |A\rangle\}$, where $|S/A\rangle = (|\sigma_1^+\sigma_2^-\rangle \pm |\sigma_1^-\sigma_2^+\rangle)/\sqrt{2}$. Since the two photons share the same frequency and spatial mode, there is no coherence between the 3×3 symmetric and 1×1 anti-symmetric subspaces[28]. We measure in six required polarization bases, chosen as $\{q, h\} = \{\frac{\pi}{4}, \frac{\pi}{4}\}, \{0, 0\}, \{\frac{\pi}{8}, \frac{\pi}{8}\}, \{0, \frac{\pi}{16}\}, \{\frac{\pi}{8}, \frac{\pi}{16}\}, \{\frac{\pi}{8}, 0\}$, to set the 10 degrees of freedom in $\rho(t_1, t_2)$. The optimization follows the Maximum Likelihood Estimate[27], where all coincidence measurements are considered. The one-photon density matrix $\rho^{(1)}(t)$ is reconstructed using the same technique. To extract the nonlinear phase from $\rho(t_1, t_2)$, we rescale for the linear dispersion and loss effects by defining the interaction matrix $\tilde{\rho}_{i,j}(t_1, t_2) = \rho_{i,j}(t_1, t_2)/\left[\rho^{(1)}(t_1) \otimes \rho^{(1)}(t_2)\right]_{i,j}$ in the basis $\{|\sigma_1^+\sigma_2^+\rangle, |\sigma_1^+\sigma_2^-\rangle, |\sigma_1^-\sigma_2^+\rangle, |\sigma_1^-\sigma_2^-\rangle\}$. The interaction matrix generalizes the standard $g^{(2)}$ definition to account for nonlinear phases and decoherence, and all

its elements are equal to 1 in the absence of nonlinearity. Figure SI3 compares the measured photon-photon correlation functions to those calculated from $\tilde{\rho}$ (see also Figure SI4). The colormaps in Fig. 2 presenting values derived from $\rho(t_1, t_2)$ have been smoothed using an unweighted, nearest-neighbor, rectangular sliding-average.

Acknowledgements

We thank H. P. Büchler, T. Pohl, J. Otterbach, P. Strack, M. Gullans, and S. Choi for useful discussions. This work was supported by NSF, CUA, DARPA, and the AFOSR Quantum Memories MURI. OF acknowledges support by the HQOC. AVG and MDL thank KITP for hospitality. AVG acknowledges funding from the Lee A. DuBridge Foundation and the IQIM, an NSF Physics Frontiers Center with support of the Gordon and Betty Moore Foundation.

[1] Scully, M. O. & Zubairy, M. S. *Quantum Optics* (Cambridge University Press, Cambridge, UK, 1997).
[2] Milburn, G. J. Quantum optical fredkin gate. *Phys. Rev. Lett.* **62**, 2124–2127 (1989).
[3] Imamoḡlu, A., Schmidt, H., Woods, G. & Deutsch, M. Strongly interacting photons in a nonlinear cavity. *Phys. Rev. Lett.* **79**, 1467–1470 (1997).
[4] Deutsch, I. H., Chiao, R. Y. & Garrison, J. C. Diphotons in a nonlinear fabry-pérot resonator: Bound states of interacting photons in an optical "quantum wire". *Phys. Rev. Lett.* **69**, 3627–3630 (1992).
[5] Shen, J.-T. & Fan, S. Strongly correlated two-photon transport in a one-dimensional waveguide coupled to a two-level system. *Phys. Rev. Lett.* **98**, 153003 (2007).
[6] Chang, D. E., Srensen, A. S., Demler, E. A. & Lukin, M. D. A single-photon transistor using nanoscale surface plasmons. *Nat. Phys.* **3**, 807 – 812 (2007).
[7] Cheng, Z. & Kurizki, G. Optical "multiexcitons": Quantum gap solitons in nonlinear bragg reflectors. *Phys. Rev. Lett.* **75**, 3430–3433 (1995).
[8] Turchette, Q. A., Hood, C., Lange, W., Mabuchi, H. & Kimble, H. Measurement of conditional phase shifts for quantum logic. *Phys. Rev. Lett.* **75**, 4710 (1995).
[9] Chang, D. E. *et al.* Crystallization of strongly interacting photons in a nonlinear optical fibre. *Nat. Phys.* **4**, 884–889 (2008).
[10] Fushman, I. *et al.* Controlled phase shifts with a single quantum dot. *Science* **320**, 769–772 (2008).
[11] Rauschenbeutel, A. *et al.* Coherent operation of a tunable quantum phase gate in cavity qed. *Phys. Rev. Lett.* **83**, 5166 (1999).
[12] Kirchmair, G. *et al.* Observation of quantum state collapse and revival due to the single-photon kerr effect. *Nature (London)* **495**, 205209 (2013).
[13] Saffman, M., Walker, T. G. & Mølmer, K. Quantum information with rydberg atoms. *Rev. Mod. Phys.* **82**, 2313–2363 (2010).
[14] Gorshkov, A. V., Otterbach, J., Fleischhauer, M., Pohl, T. & Lukin, M. D. Photon-photon interactions via rydberg blockade. *Phys. Rev. Lett.* **107**, 133602 (2011).
[15] Pritchard, J. D. *et al.* Cooperative atom-light interaction in a blockaded rydberg ensemble. *Phys. Rev. Lett.* **105**, 193603 (2010).
[16] Maxwell, D. *et al.* Storage and control of optical photons using rydberg polaritons. *Phys. Rev. Lett.* **110**, 103001 (2013).
[17] Dudin, Y. O. & Kuzmich, A. Strongly interacting rydberg excitations of a cold atomic gas. *Science* **336**, 887–889 (2012).
[18] Petrosyan, D., Otterbach, J. & Fleischhauer, M. Electromagnetically induced transparency with rydberg atoms. *Phys. Rev. Lett.* **107**, 213601 (2011).
[19] Peyronel, T. *et al.* Quantum nonlinear optics with single photons enabled by strongly interacting atoms. *Nature (London)* **488**, 57–60 (2012).
[20] Parigi, V. *et al.* Observation and measurement of interaction-induced dispersive optical nonlinearities in an ensemble of cold rydberg atoms. *Phys. Rev. Lett.* **109**, 233602 (2012).
[21] Kasapi, A., Jain, M., Yin, G. Y. & Harris, S. E. Electromagnetically induced transparency: Propagation dynamics. *Phys. Rev. Lett.* **74**, 2447–2450 (1995).
[22] Venkataraman, V., Saha, K. & Gaeta, A. L. Phase modulation at the few-photon level for weak-nonlinearity-based quantum computing. *Nature Photonics* **7**, 138141 (2012).
[23] Rajapakse, R. M., Bragdon, T., Rey, A. M., Calarco, T. & Yelin, S. F. Single-photon nonlinearities using arrays of cold polar molecules. *Phys. Rev. A* **80**, 013810 (2009).
[24] Drummond, P. D. & He, H. Optical mesons. *Phys. Rev. A* **56**, R1107–R1109 (1997).
[25] Lukin, M. D. *et al.* Dipole blockade and quantum information processing in mesoscopic atomic ensembles. *Phys. Rev. Lett.* **87**, 037901 (2001).
[26] Fleischhauer, M., Imamoglu, A. & Marangos, J. P. Electromagnetically induced transparency: Optics in coherent media. *Rev. Mod. Phys.* **77**, 633–673 (2005).
[27] James, D. F. V., Kwiat, P. G., Munro, W. J. & White, A. G. Measurement of qubits. *Phys. Rev. A* **64**, 052312 (2001).
[28] Adamson, R. B. A., Shalm, L. K., Mitchell, M. W. & Steinberg, A. M. Multiparticle state tomography: Hidden differences. *Phys. Rev. Lett.* **98**, 043601 (2007).
[29] Sevinçli, S., Henkel, N., Ates, C. & Pohl, T. Nonlocal nonlinear optics in cold rydberg gases. *Phys. Rev. Lett.* **107**, 153001 (2011).
[30] Heidemann, R. *et al.* Evidence for coherent collective rydberg excitation in the strong blockade regime. *Phys. Rev. Lett.* **99**, 163601 (2007).